Design and analysis of visible photonics resonators coated With CuO thin film

To cite this article before publication: Anshika Srivastava *et al* 2019 *Nanotechnology* in press https://doi.org/10.1088/1361-6528/ab6469

IOP Publishing Journal Title
Journal **XX** (XXXX) XXXXXX https://doi.org/XXXX/XXXX

Design and Analysis of Visible Photonics Resonators Coated With CuO Thin Film

Anshika Srivastava, Richa Singh and Shweta Tripathi*

Department of Electronics & Communication Engineering,

Motilal Nehru National Institute of Technology Allahabad, Prayagraj-211004, India

*Email: shtri@mnnit.ac.in

Abstract

The optical and structural properties of CuO film deposited on n-Si via spin-coating method has been accomplished for diverse anneal time. All the characterization was made by using x-ray diffraction (XRD), field emission scanning electron microscopy (FESEM), UV-Vis spectroscopy, ellipsometry spectroscopy and photoluminescence. The detailed analysis unveiled the favorable behavior of CuO film for visible photonics resonators such as fabry-perot and ring resonators. The best suitable property was obtained for 15min annealed film. Accordingly, CuO film coated resonators were simulated and analyzed theoretically using MODE Solutions tool by Lumerical and MATLAB. In fabry-perot resonator, the transmission intensity, contrast factor and finesse has been computed for different anneal time and incident angle of light incidence. Further for CuO ring resonator, the eigenmode solver was incorporated (in the wavelength range 300-900 nm) to compute, effective refractive index, propagation constant, group velocity, losses, dispersion and transmission intensity. Additionally, utilizing the basic expressions, free spectral range, full-width at half-maximum and quality factor was derived.

Keywords— Optical microcavity, Copper Oxide Thin Film, Fabry Perot Resonator, Ring Resonator.

1. Introduction

Optical microcavities have become a prominent field of research in the recent past due to their high quality factor, unique resonant and geometrical properties [1-3]. The basic principle of operation of optical microcavities involves confinement of light by making use of repetitive resonant circulation. Unlike conventional optical structures that makes use of mirrors to confine light, optical microcavities relies on dielectric coatings or optical band gap systems to achieve total internal reflection and thereby the confinement of light [4-5]. Application and appeals of optical microcavities have brought forth a new generation of on-chip optical devices [6]. Nowadays devices based on optical microcavities, such as lasers, optical filters, sensors and diodes, are being investigated [6-8]. Since the main operation of optical microcavities makes use of total internal reflection phenomenon, that is dependent upon the reflectance of the cavity coating therefore, thin film coating with appreciably high reflectance have become essential requirement for optical microcavities [9-10]. Further, with the focused approach of scaling optical devices to desired cavity dimensions such that appreciable performance is maintained, is vital to realize. Material selection for cavity coating plays an important role in deciding aforementioned parameters. Semiconductor material attracts tremendous attraction as a thin film coating material for optical microcavities, since they can depict active as well as passive nature in a single material itself [11-12]. CuO is a semiconductor material known for its well established optical performance [13-14]. It can be used to support desired resonant modes in an optical microcavity. High reflectance, a highly favored attribute of

Copper oxide, has been well exploited in optical microcavities [15].

Despite the fact that an excellent development has been made in the low-loss integrated photonics at telecom wavelengths yet visible wavelengths has got less attention. Visible photonics finds application in several fields such as optical imaging, ontogenetic etc. In the present paper one of the main components of integrated photonics i.e. resonators have been considered for design and analysis purpose. Mainly there are two classes of resonators first is standing wave resonator, and second is travelling wave resonators. A Fabry-Perot resonator is a linear resonator belonging to standing wave category of optical resonators. It consists of two highly reflecting mirrors and is frequently used as a high-resolution optical spectrometer [16]. Optical ring resonator is travelling wave type resonator, it do not require facets or gratings for optical feedback, making them particularly suited for monolithic integration. The filtering property shown by the ring resonator has led to an advancement in optical signal processing, detection of bio particles, telecommunication and laser applications [17].

In the present paper, the first section represents the brief introduction involving the formerly recounted work in the field of optical microcavity. Then after, the experimental procedure followed for CuO film formation has been illustrated. Subsequently, the structural and optical analysis of the deposited CuO film was performed, using a number of characterizing instruments. Further regarding application implications, we have demonstrated the outcomes of CuO film resonators such as fabry-Perot and ring resonators. At last we have discussed the summary of this work.

2. Experimental Details

In the present work, copper oxide thin film was deposited on n-Si (100) substrate by sol-gel spin coating technique. In order to prepare copper oxide sol, copper (II) acetate was used as a starting material. In order to obtain the sol, 20ml of 2-methoxyethanol was added to 1ml of ethanolamine under constant stirring. After this, 1.09 g of copper (II) acetate was added, that was dissolved completely after 10 minutes of stirring and deep blue solution was formed. These all steps were carried out at room temperature. The sol was placed at room temperature to be aged for at least 2 days before it could be used to synthesize the CuO nanostructure. At first, the n-type Si substrate was cut into small stripes of size $0.75'' \times 0.75''$ and the substrate pieces were thoroughly cleaned by using steps prescribed by RCA-1 and RCA-2 process to remove the organic and ionic contaminants, respectively. After thorough cleaning, Si substrates were immediately employed to synthesize CuO thin film from CuO sol-gel using spin coating technique. At first, Si substrate was preheated for 10min on the hot plate and then mounted on the sample holder of the spin coater. Subsequently, the sol was poured drop by drop on substrate and sample holder was rotated at a speed of 2000 rpm for 45seconds. After each cycle of spin coating, the substrate was post-dried at 373K for 5min to evaporate the solvents and obtain the stable film. This process was repeated several times, 6 cycles of the process yielded the average thickness of 108 nm of as-grown CuO layer. Then, the deposited film was annealed at 723 K for 5, 15 and 25min, respectively.

3. CuO Thin Film Analysis

Annealing provides structural improvisation, and surface roughness control in thin film that are qualitatively represented by alteration in microstructure and phases present in the film. The prominent changes in the property of film are generally visible in terms of decreased FWHM, dislocation density and strain whereas crystallite size is increased. As we tend to increase the annealing time or increase the annealing temperature, the smaller crystallites of the film absorbs more thermal energy and start fusing with each other and thereby resulting in bigger crystallites. These microstructural and phase changes directly affect the optical properties exhibited by the film. For instance, in general case, the optical band gap of thin film increases with annealing, due to the reduction of crystal defect. Likewise absorption property of the film is also affected on annealing due to the roughness variation caused by restructured morphology. Due to the variation in absorption parameter, the refractive index of the film also changes. In addition to this, it is also well known that absorption improves the generation and recombination rate of generated electron-hole pairs (EHPs) that helps in the light emission. Therefore, indirectly PL intensity is also affected by the variation in annealing time. As discussed above the variation in annealing time is expected to induce significant variation in optical properties of the film. In order to observe the same the deposited film thickness and optical band gap of CuO films were evaluated using variable angle spectroscopic ellipsometer. Surface morphology and crystalline quality of as-grown CuO samples were investigated using FESEM (JEOL JEC-3000 FC) and X-ray diffraction spectroscopy (Rigaku smart lab in-plane grazing angle XRD).

3.1 Structural Analysis

With an intention to examine structural morphology of CuO film on n-Si substrate annealed for different time intervals, x-ray diffraction (XRD) patterns have been recorded for all annealed films (as depicted in fig. 1). Peaks along the different orientation in 5min sample demonstrate the polycrystalline monoclinic nature of the CuO film in tenorite phase. The presence of the CuO film is recognized from the standard JCPDS card number 00-005-0661. But in 15min and 25min sample at some distinct orientation such as (020) and (220) the peak splitting can be observed. This peak

splitting is due to the presence of Cu_2O peak as signposted by (*) in fig. 1. The presence of the Cu_2O peak is confirmed by JCPDS card number 01-073-6237. Increment in the annealing time, intensifies the peak in the same orientation. This signifies that the atom growth upsurges in those directions by an unaffected polycrystalline structure. With the obtained XRD pattern we have determined the full-width at half maxima (FWHM) as given in table. I The value of FWHM designates the stress/strain in the film that are nevertheless created by the mismatch of lattice between film/substrate, anneal time, deposition temperature etc. The strain present in thin film makes diffraction peak wider that results in reduced crystallite size growth. We can comprehend here that 25min annealed sample shows less FWHM. This specifies low strain between the molecules of the crystal structure at high anneal time.

It is noteworthy here that FWHM in XRD of thin films gets influenced by the stress/strain present due to the lattice mismatch between the substrate and the film. Moreover we have calculated the average crystallite size at 5min, 15min and 25min annealed CuO by using the eminent Debye-Scherrer formula (eq. 1) [18].

$$D = \frac{k\lambda}{(FWHM)\cos\theta} \tag{1}$$

where FWHM is in radians, 'λ' the X-ray wavelength that is equal to 1.5405 Å, *'k'* is the constant with value of 0.9, *'D'* represents the crystallize size in Å of the plane upright to the lattice planes for the observed reflection and *'Θ'* the Bragg's angle. The attained values of crystallite size for different anneal time for each *(hkl)* plane is given in table I and II. It can be illustrated that 5min annealed CuO film has minimum crystallite size and 25min has maximum crystallite size. It can be observed from the table. I that crystallite size has an inverse relation to FWHM of the diffraction peak of diffractogram. Now with the help of crystallite size we have determined the dislocation density from eq. 2 [19], caused by the imperfection growth, lattice mismatch or stress/strain. We have witnessed here that as the anneal time is increased from 5min to 25min, the dislocation density or the disruption in the film reduces. This resembles to a more systematic crystallite arrangement.

$$\delta = \frac{1}{D^2} \tag{2}$$

Now eq. 3 specifies the texture coefficient of the film in order to recognize the orientation of growth in a certain direction [20-21]. Texture Co-efficient,

$$TC(hkl) = \frac{N\left(I_o / I_c\right)}{\sum_{i=1}^{N} I_o / I_c} \tag{3}$$

Here Io is the measured intensity from the X-ray diffraction spectroscopy, Ic is the intensity of a generic peak for an entirely random sample specified in JCPDS card number 00-005-0661 and N is the total reflections deliberated in the study.

In table. I we have deliberated the *TC (hkl)* for different anneal time CuO film. It was detected that TC is preeminent for all the samples in (112) direction. As per the literature the value of TC decides the preferred orientation of the atom growth. It was said that if the value of TC>1 then that orientation would be the favoured one [22]. We can observe from the table that in (112) plane TC is much higher than one, thus it is most suitable orientation among all. Plane (020) will also be favoured for 15min and 25min samples for value of TC>1. The highest value of TC is found in 15min sample for (112) plane. Therefore 15min annealed CuO would be preferable among all.

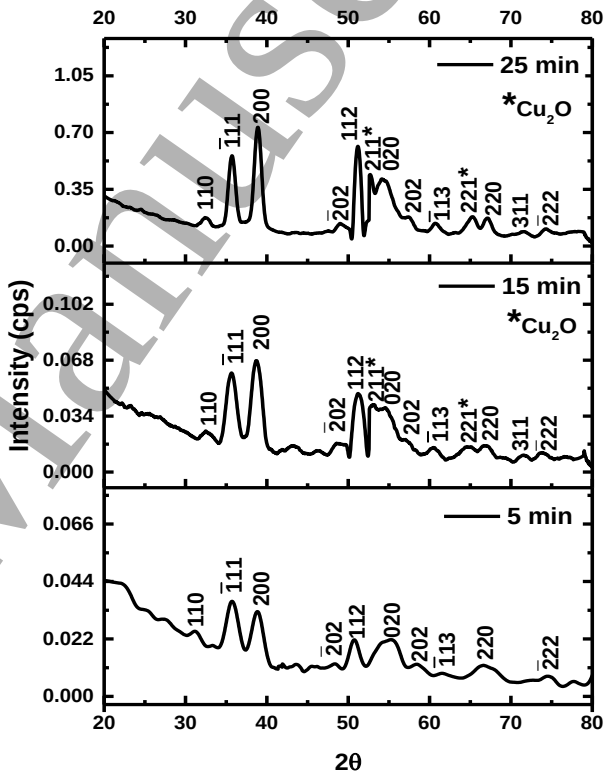

Fig. 1. XRD spectrum of CuO film for different annealed time.

Subsequently, for the purpose to measure the lattice parameters of CuO film monoclinic structure, the inter-planar distance *'d'* (Å) between two successive planes has been calculated. For that we have utilized Bragg's formula as indexed in eq. 4.

$$n\lambda = 2d\sin\theta \tag{4}$$

Here *n=1* is a positive integer. And the lattice constraints *a, b, c* and γ are premeditated from eq. 5, that is specific for monoclinic structure [23].

$$\frac{1}{d^2} = \frac{h^2}{a^2\sin^2\gamma} + \frac{k^2}{b^2\sin^2\gamma} - \frac{2hk\cos\gamma}{ab\sin^2\gamma} + \frac{l^2}{c^2} \tag{5}$$

TABLE I
Properties extracted from XRD spectrum for diverse anneal time

S.N	Planes (hkl)	Space, d (Å)	Properties	Anneal Time (minutes)		
				5 min	15 min	25min
1.	-111	2.523	FWHM (radians)	0.0433	0.0297	0.0198
			D (Å)	33.5804	48.9083	73.2718
			TC	0.0141	0.0138	0.0107
			δ (10^{16}/m^2)	8.8680	4.1805	1.8626
2.	200	2.312	FWHM (radians)	0.0370	0.0287	0.0194
			D (Å)	39.6919	51.1281	75.7081
			TC	0.4107	0.5280	0.4738
			δ (10^{16}/m^2)	6.3474	3.8254	1.7446
3.	-202	1.866	FWHM (radians)	0.0851	0.0386	0.0355
			D (Å)	17.8582	39.2994	42.8344
			TC	0.1893	0.1626	0.1064
			δ (10^{16}/m^2)	31.3562	6.4748	5.4502
4.	112	1.778	FWHM (radians)	0.0309	0.0270	0.0157
			D (Å)	49.4940	56.7598	97.6587
			TC	4.0952	5.8283	5.5124
			δ (10^{16}/m^2)	4.0822	3.1039	1.0485
5.	020	1.714	FWHM (radians)	0.0478	0.0351	0.0211
			D (Å)	32.6296	44.3241	73.4939
			TC	0.9749	1.1709	1.0272
			δ (10^{16}/m^2)	9.3923	5.0900	1.8513

TABLE II
Crystallite size and lattice parameter for diverse anneal time

S. No.	Anneal Time (minutes)	Average Crystallite Size (Å)	Lattice Parameters
1.	5min	34.6508	a= 5.8383 Å, b=4.3282 Å, c=4.8831 Å , γ =97.61^0
2.	15min	48.0839	
3.	25min	72.5934	

Fig. 2 witnesses the effect of annealing time on the thickness of CuO film. This measurement has been performed by using variable angle ellipsometry spectroscopy. It can be illustrated from the graph that anneal time has a direct influence on the film thickness. This can be associated with the crystallite size of the film. As discussed in XRD result, anneal time stimulates the recrystallization process in the film and thus upsurges the crystallite size. It was also conferred in XRD pattern that on making the large intervals for annealing, the average crystallite size upsurges. For that reason, it is fairly recognizable that whole thickness of the CuO film will increase as well. The large thickness plausibly reflects presence of higher compressive stresses in the film that indicates mean tensile stress is lower during crystallite growth, therefore resulting in a higher crystallite size. The compressive stress is neutralized by the tensile stress giving rise to the fact that larger the compressive stress present during the growth, higher will be eventual crystallite size.

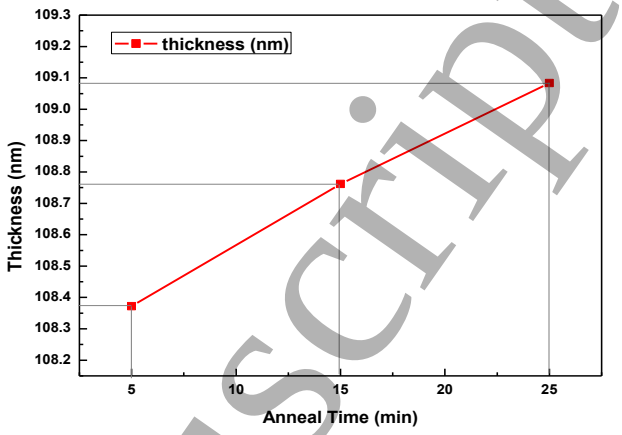

Fig. 2. Variation of CuO film thickness with annealing time at constant temperature.

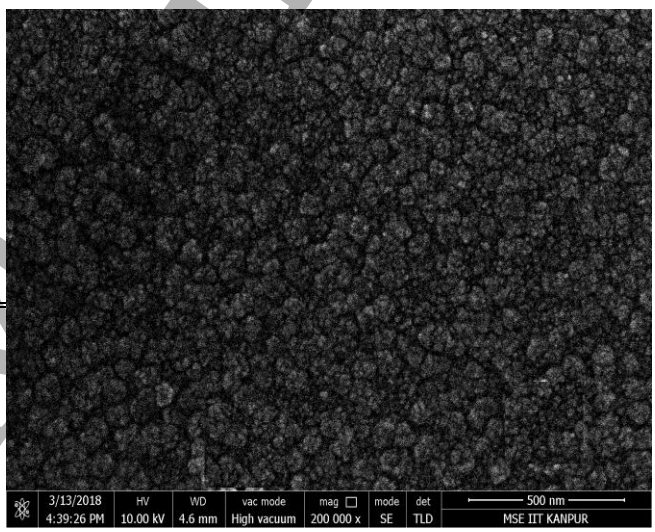

(a)

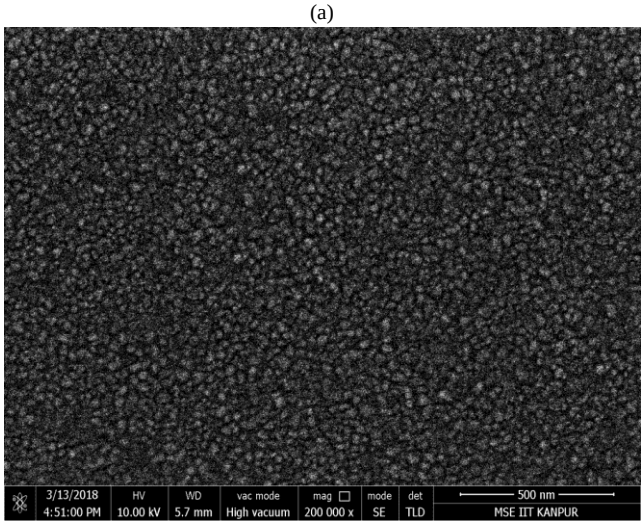

(b)

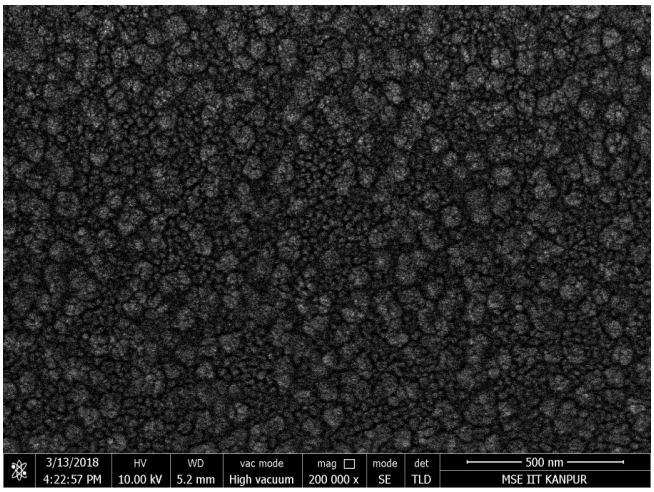

(c)

Fig. 3. FESEM image of CuO annealed film for (a) 5min (b) 15min (c) 25min

In fig. 3 the surface morphology of the CuO film annealed at different time was observed through the FESEM images. The morphology of the surface validated the even deposition over the complete n-Si substrate. We found that at 5min anneal interval the dimension of grains are larger whereas at 15min all the nano-sized grains fades. It might be due to the overall recrystallization effect. And at 25min anneal time the large unsystematic and consistently distributed condensed nano-sized grains are formed that can be the cause of increased thickness (as substantiated from the ellipsometry data). A single grain can enclose several domains with diverse orientations and therefore the size determined with FESEM is always expected to be larger than determined by XRD. This is also evident from the results shown in table III. Small sized grains are present in 15min annealed sample that can be possibly due to the reduced amount of surface roughness.

TABLE III
Properties extracted from FESEM image for diverse anneal time

S. No.	Anneal Time (minutes)	Average grain Size (nm)	Average grain Area (nm^2)
1.	5min	73.0649	100.6209
2.	15min	24.17	34.5143
3.	25min	76.3759	107.1293

3.2 *Optical Analysis*

The optical study of the film evaluates its interaction with the light beam. When the light (electromagnetic wave) interacts with the film surface, some of the amount gets reflected and some of it gets transmitted. The information of the electronic states is carried by the reflected wave. The light energy that passes into the film further creates some absorption, scattering and transmission. The energy from the absorbed radiation can be dissipated or re-radiated as photons of dissimilar frequencies. This behavior permits the material to be used for a number of applications that are very crucial to be identified. Thus, with the aim to express the optical implication of the film, we have examined various properties such as reflectivity, refractive index, extinction co-efficient, absorption coefficient, band-gap and photo-luminescence. All the parameters have been evaluated from ellipsometry in the wavelength range of 300-900 nm. The glossiness of the surface can be understood by evaluating reflectance property of the film. For that purpose, we have depicted in fig. 4 the dependency of reflectance on the wavelength for different angle of incidence, using spectrocopic ellipsometry.

In fig. 4 we have compared reflectivity's at 50^0, 60^0, 70^0 and 80^0 angle of incidence for all different time annealed film. It can be noted from the graph that 15min annealed CuO film depicts maximum reflectivity (≥80%) for the given wavelength range and angle of incidence. This behavior can also be corroborated from the FESEM images, as for 15min annealing time, the surface is comparatively smooth with surface roughness of 3.78nm (table. IV), hence better reflectivity. Thus, it is worth to mention here that 15min CuO film have great appropriateness for optical devices containing mirror like surface.

Now, since the microroughness casts the basis of the optical losses therefore it is essential to optimize the semiconductor coating morphology for the optimum roughness which can critically be achieved through the variation in annealing time. Therfore, keeping in view this fact, surface roughness of 15min annealed CuO film has been compared with some already reported coatings for waveguiding applications [24-27]. It can be seen from table. IV, the surface roughness of 15min annelaed film is 3.78 nm, which is lower than some of the results reported for waveguiding applications.

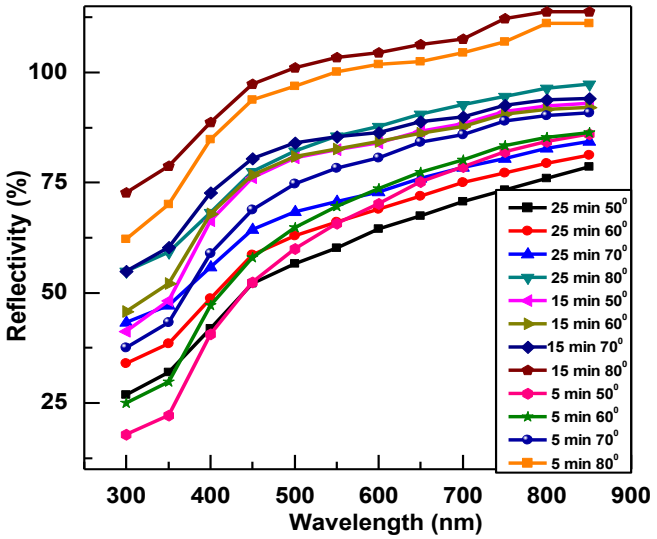

Fig. 4. Reflectivity vs. wavelength for different anneal time and angle of light incidence.

TABLE IV
Surface Roughness determined from AFM results and compared with some published results

S. No.	Waveguiding Layer	Surface Roughness
1.	Brass sheet [24]	40 nm
2.	Aluminium sheet [24]	30 nm
3.	SOI [25]	5 nm
4.	SOI [26]	5 nm
5.	SOI [27]	13.5 nm
6.	1 mol% Er-doped ZnO [5]	0.16 nm
7.	15 min annealed CuO film	3.78 nm

The variation of refractive index with wavelength is shown in fig. 5. It can be observed that the refractive index changes moderately with wavelength for 5min and 25min annealed samples, however it becomes almost constant (for wavelengths greater than 600nm) for 15min annealed sample. It clearly indicates that Fresnel losses will be less in the starting of visible wavelength region and then increases with increase in wavelength yet 15min annealed sample faces almost constant loss after 600nm wavelength.

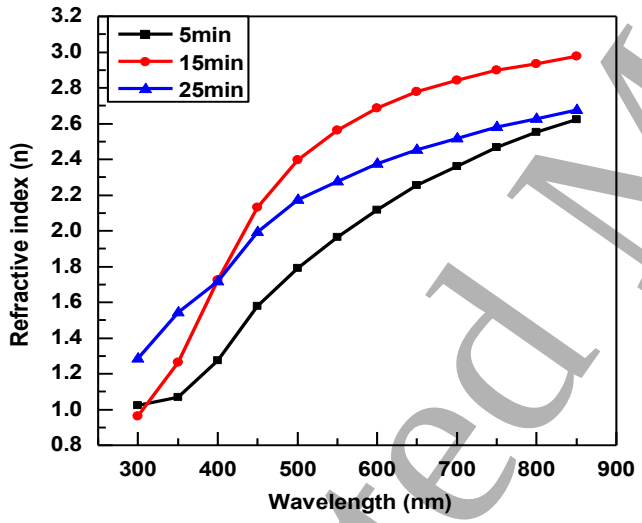

Fig. 5. Refractive index vs. wavelength for different anneal time

The absorption coefficient variation with respect to wavelength is represented in fig. 6. It was observed from the result that absorption of CuO thin film is high in the ultraviolet region and gradually decays in visible region of electromagnetic spectrum of light for diverse annealing time. There is clear distinction in the intensity of absorption coefficient for diverse annealing time, with 25min film exhibit higher absorption coefficient. This can be attributed to the relative thicker 25min annealed CuO film that triggers the absorption. On the other hand, film annealed for 15min displays higher absorption value than 5min annealed film for wavelength range of 300-600nm. However for higher wavelength values absorption of 15min annealed film suppress due to formation of smoother surface as reflected by the FESEM image (fig. 3(b)).

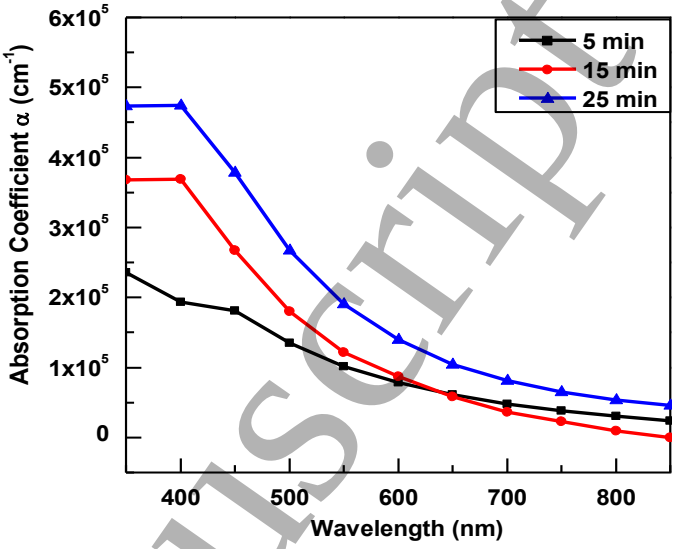

Fig. 6. Absorption coefficients vs. wavelength for different anneal time

Now we have considered the optical energy band-gap of different time annealed samples. This is a vital parameter for the evaluation of light that can be reflected or absorbed by the material. It implies that the incident light energy greater than or equal to optical band-gap will get absorbed. We have evaluated this parameter via utilizing the relation given in eq. 6 [28].

$$\alpha = \frac{C(h\upsilon - E)^n}{h\upsilon} \quad (6)$$

Here 'E' is the optical energy band-gap, 'C' is constant, 'n' implies the method of transition, 'hυ' is the energy of photon. Now for the evaluation purpose we have plotted variation of $(\alpha h\upsilon)^2$ against hυ as shown in fig. 7.

From fig. 7, we recognize that 5min CuO film is showing only one linear segment whereas 15min and 25min sample is showing two linear segments. The two linear segments correspond to band gap range for 15min and 25min sample. The bandgap range for 15min annealed film is (2.39-2.96) eV and for 25min annealed film is (2.28-2.74) eV. It can be observed that 15min sample is showing wide range of optical energy bandgap among all. In case of single phase presence (i.e CuO), it is expected to be single linear segments at the low energy position, while the presence of mixed phase, impurity or any defects can generate new sub level which can be the reason for getting two linear segments. As discussed in XRD result, peak splitting is observed in 15min. and 25min. annealed sample giving rise to mixed phase presence of CuO and Cu_2O.Therefore, two linear segments in Tauc plot are due to the presence of mixed phase of CuO and Cu_2O. Further, there is a noteworthy reduction in optical band-gap, as we increase the anneal time. The reason for this behavior is the shift of absorption coefficient edge towards

high wavelength in the visible range [29].

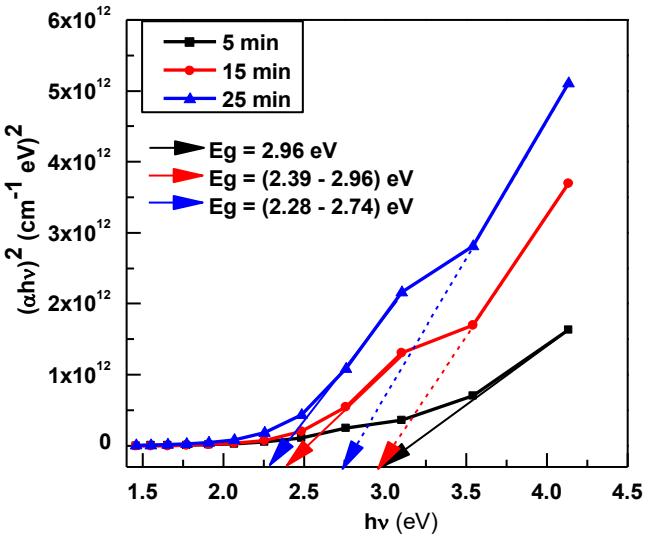

Fig. 7. Optical bandgap of CuO thin film annealed at 450^0 C for 5 min, 15 min and 25 min.

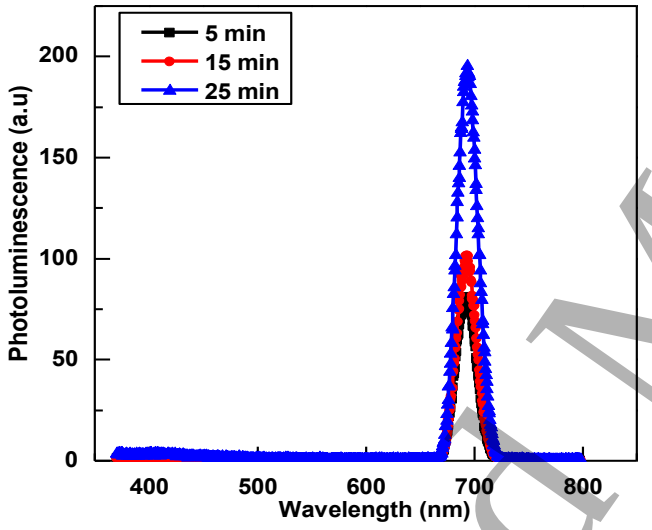

Fig. 8. Photoluminescence vs. wavelength plot of CuO film at different anneal time

Fig. 8 shows photoluminescence intensity of CuO thin film. It can be depicted from the graph that the film annealed for 25min, indicates larger PL intensity, this may be due to the fact that 25min annealed CuO film exhibits higher absorption coefficient (shown in fig. 7) that causes an enhancement in generation and radiative recombination rate of electron-hole pair. Further, 5min annealed sample shows least PL intensity because the lower absorption coefficient and the presence of non-radiative traps that depresses the direct transition of electron from conduction band to valence band. As the annealing time of CuO thin film plays a crucial role in formation of surface defects that creates radiative and non-radiative recombination center within the band-gap of the material.

3.3 *Analysis of Fabry Perot Resonator and Ring Resonator for Visible Photonics*

Integrated photonics is an influential step to increase the performance and dependability of optical frameworks with cost effective and scalable options for free-space optics. While incredible advancement has been made in the field of low-loss integrated photonics at telecom wavelengths, visible wavelengths has got less consideration. However, numerous applications such as optical imaging, opto-genetics etc., use visible or near visible wavelengths. As of now, analysis of optical coatings for visible wavelength has been very less implemented and researched. The magnificence of optical coatings relies in the fact that one can engineer their performance by selecting appropriate deposition method and material. In particular three classes of optical coating exists i.e. dielectric, metal, and semiconductor. When light enters into dielectric material electrons adds to their vibration and thereby the light slows down, yielding an index of refraction greater than unity. Since there is no absorption phenomenon therefore dielectric coatings are considered to be a better option for antireflection coating applications. However, in metals, light is absorbed quickly giving rise to high reflectance as well, consequently metals serves as better mirror coatings. In semiconductor coatings, semiconductors act like dielectric thin films with high refractive indices at longer wavelengths and for shorter wavelengths it behaves like metal coating. Any optical coating preliminary uses Snell's law of refraction and light reflection at the coating interface as it main operating principle. Snell's law determines how the optical coating properties changes with the angle of the incidence whereas reflection changes with the thickness of the coating. The thickness of semiconductor coating can be well controlled and stabilized by using appropriate deposition method and annealing technique. Therefore, as it seems and so researched in the literature about the semiconductor coating quality to determine overall performance of the optical device. Other important parameters of the optical devices that depend on the semiconductor coating quality are reflectivity and ultralow optical losses from scatter and absorption, low mechanical loss, and high thermal conductivity. Among a number of semiconductors, the material to be chosen should have aforementioned properties, CuO fits well in this bracket [2, 5]. The reflectivity of CuO film can be enhanced that enables it to be very useful candidate for use in optical microcavities. In the present paper it is successfully demonstrated with the results that reflectivity of annealed CuO film is very high for the wavelength range of 400-800nm. Thus we came to the conclusions that annealed CuO film can be used as an optical coating material for ring and fabry-perot resonators.

In the present section we will analyze performance of Fabry Perot resonator and ring resonator coated with CuO thin film, for visible photonics.

3.3.1 *Fabry-Perot Resonator*

An optical cavity causes light proliferation in a closed path through several reflections from two or more existing mirrors. Basically, there are two types of resonators characterized by its wave nature: standing wave (or Fabry-Perot) resonator and travelling wave (or ring) resonator. Ring resonator generally has a minimum of three mirrors whereas Fabry-Perot (FP) resonators consists of two mirrors arranged parallel to each other. In 1899 a Fabry-Perot resonator was devised that confirmed its ability in incalculable spectroscopic applications due to its high finesse property [30]. Afterwards in 1960, it became a fundamental root for enormous class resonators that permits laser oscillations. FP resonator shows small transmission with sharp resonance [16]. The light incident on the surface of the resonator mirror gets reflected and makes several round trips inside the cavity. Multiple light waves departing from the cavity interact with one another and forms an interference pattern on the detecting screen. The variation in the function of transmission occurs by the interference of several reflections within both mirrors. When the transmission rays are in same phase, the constructive interference occurs that resembles to high amplitude transmission peak. If transmission rays are in different phases then it gives rise to a destructive interference (minimum or small amplitude transmission). This in-phase and out-of-phase behavior of transmission is governed by the wavelength (λ) of the propagated light in vacuum, resonator thickness (t), incidence angle of light (θ) and the material refractive index with the cavity (n). Now the difference in phase between each successive reflection can be given by eq. 7 [16].

$$\delta = \left(\frac{2\pi}{\lambda}\right) \times 2nt\cos\theta \tag{7}$$

Now if the both the reflecting surface of the FP have reflectance 'R_{fp}' the transmission intensity of the FP resonator can be illustrated as [16]

$$T_{fp} = \frac{\left(1-R_{fp}\right)^2}{1+R_{fp}^2-2R_{fp}\cos\delta} \tag{8}$$

From the above eq. 8, it can be said that transmission intensity is highly dependent on the reflectivity of the mirror that are coated with some reflecting material. Therefore for high transmission intensity and less propagation loss it is vital to analyze the material property to be coated on the reflecting surface. Since in the above section it was clearly seen that 15min annealed CuO thin film on n-Si substrate shows promising reflectance, therefore in this section we have elaborated the performance of FP resonator made with CuO thin film. Fig. 9 shows the schematic of Fabry-Perot resonator that is basically formed by two parallel highly reflective CuO thin coated on silicon substrate. The distance between the parallel mirrors is 'D'. The parameters scrutinized for the study purpose of CuO film based FP resonator are transmission intensity, finesse and contrast factor.

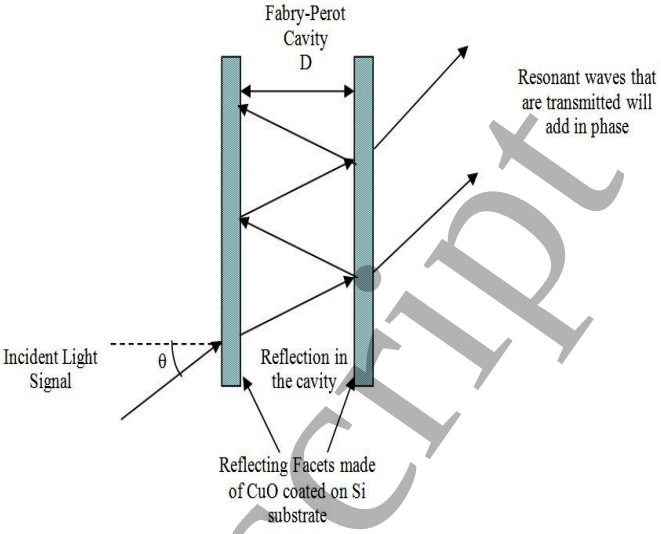

Fig. 9. Schematic Diagram of Fabry Perot resonator cavity

3.3.1.1 Transmission Intensity of Fabry-Perot Resonator

Since the reflectivity of CuO films annealed for different anneal time varies subsequently with wavelength, therefore, it will make a notable influence on the transmission intensity of light beam (given in fig. 10). With such determination we have examined the transmission intensity of the light travelling through the CuO thin film coated FP resonator in the visible region of wavelength. Firstly, in fig. 10 we can see there are disordered variations in the transmission intensity for 5min, 15min and 25min CuO coated FP resonator. The disordered transmission intensity relies upon the losses, propagation constant and the distance between two reflecting mirrors. The disordered feature of transmission intensity may prove to be a significant mechanism for secured optical communication applications. This disordered feature is hard to achieve in optical regime as perfectly reflecting coating do not exist. Basically, there are two main requirements for the disordered transmission system for secured communication: (a) resonator should have exponential sensitivity that can be achieved by unstable reflecting mirrors, (b) confinement of light for large duration that can be achieved by stable reflecting mirrors. Here we can see there is an exponential variation of transmission intensity with wavelength. Consequently, for different anneal time the disordered pattern varies, i.e. exponential sensitivity is more in 5min and 25min sample whereas it is less in 15min sample. But there is a stability in the transmission peaks of 15min annealed CuO film. Therefore, 15min annealed sample is highly stable with favorable sensitivity when compared to others. Thus, variation in anneal time can possibly lead to a secured optical commination that can also be tuned. The peaks of the transmission intensity reflects the location of passbands that occurs at $N\lambda=2nD$, where 'N' is an integer, 'n' is the refractive index of the CuO thin film

and 'D' is the distance between the mirrors. For same angle of incidence, passband peaks are sharper for 15min annealed film. The distance of two consecutive passbands is known as free spectral range (FSR) and FSR changes significantly with the annealing time. Another significant parameter is full width of the passband at half maximum value that is known as FWHM (full width half maximum) that determines number of wavelengths that can accommodate in the FSR. An approximation of the number of wavelengths that can be accommodated in the resonator can be obtained by the ratio of FSR to FWHM. This ratio is also known as finesse, through which we can determine the confinement of light for a number of round trips into the waveguide of fabry perot resonator (that we will discuss later). Since the structure of the passbands is being affected by the annealing time of the CuO film therefore number of wavelengths that resonator can support is indirectly dependent upon the annealing time of the film.

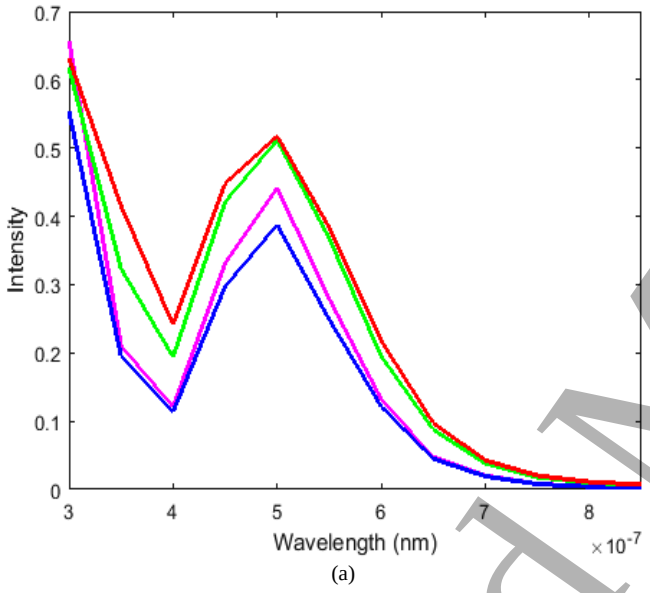

(a)

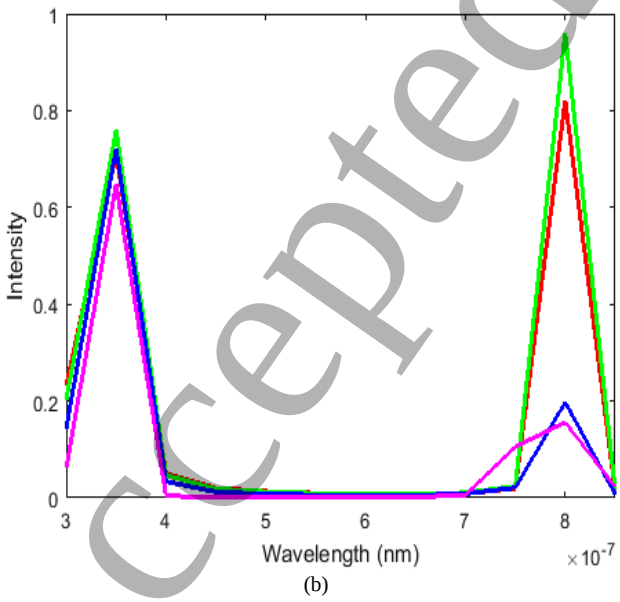

(b)

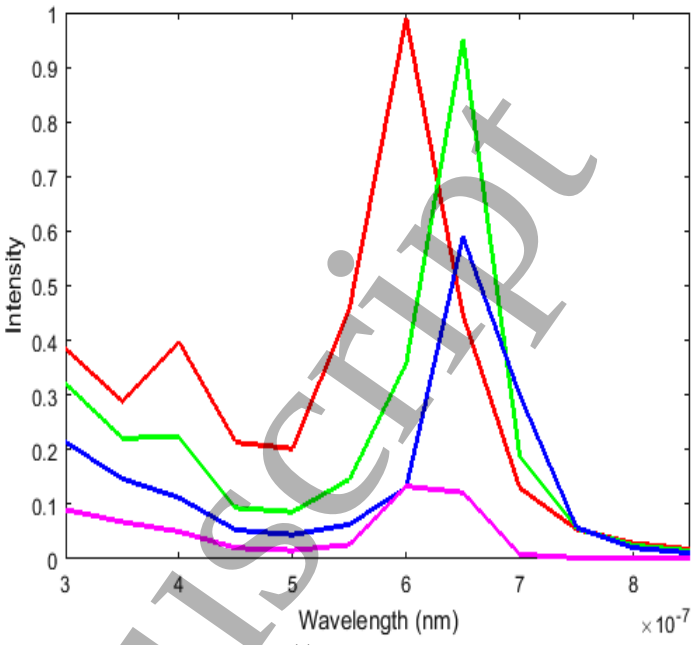

(c)

Fig. 10. Transmission intensity variations with wavelength at different angle of incidence for (a) 5min, (b) 15min and (c) 25min CuO film on Si-substrate. Red, green, blue and pink coloured lines are indicating 50^0, 60^0, 70^0 and 80^0 angle of light incidence, respectively.

3.3.1.2 Finesse of Fabry-Perot Resonator

As discussed earlier finesse (F_{fp}) is a crucial parameter to be recognized in order to enumerate the behavior of CuO FP resonator. Theoretically, finesse defines the total sum of light rays getting interfered inside the FP optical cavity. It implies that high value of finesse will indicate large amount of interfering rays i.e. a more comprehensive interference process will occur. This will result in a fascinating resolution capability. The finesse of CuO coated FP microcavity can be given by eq. 9 [31].

$$F_{fp} = \frac{\pi\sqrt{R_{fp}}}{1-R_{fp}} \qquad (9)$$

From the above equation it is clear that finesse factor has a large dependency on the reflectivity of the two parallel arranged mirrors. It is for the reason that reflectivity of the mirror has a straight impact on the amount of beam that will oscillates inside the cavity. Additionally, there are some other factors like surface morphology and stability of the resonator that bounds the finesse of CuO FP resonator [32]. In table V, the variation of finesse with respect to reflectivity has been graphically represented for different angle of incidence and annealing time. It can be seen that finesse rises with the reflectivity of the mirror (as evident from fig. 4) i.e. high reflecting surface will result in good interference of multiple beams in the cavity.

TABLE V
Finesse for diverse anneal time and angle with respect to mirror reflectivity R

R	Finesse											
	5min				15min				25min			
	50⁰	60⁰	70⁰	80⁰	50⁰	60⁰	70⁰	80⁰	50⁰	60⁰	70⁰	80⁰
0.3	2.59	2.47							2.50	2.60		
0.4	3.40	3.46	3.54	3.60					3.41	3.46	3.51	
0.5	4.59	4.53	4.67	4.19	4.81	4.60	4.94		4.50	4.50	4.38	
0.6	6.00	6.26	6.16	5.88	6.70	6.67	6.30		6.13	6.10	6.21	5.66
0.7	8.88	9.43	9.02	8.63	9.21	9.51	9.05	8.99	8.78	8.93	8.79	8.69
0.8	14.29	14.46	14.93	14.02	14.65	14.67	14.95	14.28	12.58	13.88	14.35	13.64

3.3.1.3 Contrast Factor of Fabry-Perot Resonator

Likewise finesse another vital constraint; contrast factor (C_{fp}) has direct reliance on the mirror reflectivity of CuO FP resonator. Conceptually, contrast factor elucidates the maximum to minimum transmission ratio. If it is high that will infer less transmission losses in the resonator. Contrast factor can be related with reflectivity as well as to finesse by eq. 10 and eq. 11 [16].

$$C_{fp} = \left(\frac{1+R_{fp}}{1-R_{fp}}\right)^2 \tag{10}$$

$$C_{fp} = 1+\left(\frac{2F_{fp}}{\pi}\right)^2 \tag{11}$$

In table VI the variation of contrast factor with respect to reflectivity have been vividly signified. It can be seen that contrast factor rises with the reflectivity of the mirror i.e. maximum to minimum transmission ratio is high in the cavity. The contrast ratio as high as 30000 has been obtained for 15min annealed CuO FP resonator.

TABLE VI
Contrast Factor for diverse anneal time and angle with respect to mirror reflectivity R

R	Contrast Factor											
	5min				15min				25min			
	50⁰	60⁰	70⁰	80⁰	50⁰	60⁰	70⁰	80⁰	50⁰	60⁰	70⁰	80⁰
0.3	3.63	4.22										
0.4	5.45	5.64	2.03	6.03	4.80				4.76			
0.5	8.18	11.10	8.12	10.05	8.90	11.14			8.23	9.33		
0.6	15.45	17.56	14.21	20.10	18.30	19.33	16.47		14.87	16.00	16.33	
0.7	30.90	34.13	28.42	132.16	35.24	35.91	33.30	151.51	30.65	31.55	32.51	31.91
0.8	82.72	80.99	81.21	284.42	83.83	82.87	82.67	303.03	65.13	80.00	80.102	31.92

3.3.2 *Ring Resonator*

The investigation of section 2 makes available a passageway to use CuO thin film coating in optical devices, such as resonators. With such enthusiasm we have designed and simulated ring resonator based on CuO film of different anneal time within this fragment of work. An optical ring resonator entails a set of waveguides. One of them is encompassed to couple the light within the bounds of the resonator, while the other waveguide is used to extract the light outside of the ring resonator [33]. Additionally, a ring molded closed-hoop is situated between the above-mentioned waveguides. This ring inside the waveguides serves as a filter that permits the light of resonant wavelength. And these permitted lights accrual their intensity via constructive interference.

In the designed optical ring resonator the core of the waveguide is assumed to be silicon [11] whereas the cladding is made up of CuO thin film. Now as we know that when the light is incident on an interface separated by two different medium with incident angle greater than the critical angle, then without any major loss it can travel over a significant distance. The critical angle can be defined as the angle of incidence beyond which total internal reflection (TIR) come about. It may well specified by [34] in eq. 12.

$$\theta_c = \sin^{-1}\left(\frac{n_2}{n_1}\right) \quad (12)$$

For the CuO-coated optical waveguide, 'n_2' denotes the refractive-index of CuO film (for the reason that light is exposed on the same) and 'n_1'denotes the refractive-index of the silicon present within the waveguide. Since, $n_1 > n_2$, the state of TIR would occur and light will travel through the waveguide without any substantial loss. Critical angle as evaluated for 5min, 15min and 25min annealed sample respectively, lies in the range of ~12.5°-45° , ~15° -55° and~17.5° -47.5°.In this range of critical angles, lower limit is critical angle at 300nm wavelength, and upper limit is critical angle at 850nm wavelength. So, if in the proposed resonator light is incident at some angle greater than critical angle then total internal reflection will take place. As evident from reflectivity results of CuO thin film for different angle of incidence each being greater than critical angle of the proposed resonator, 15min annealed CuO film seems to the best suitable option owing to its high reflectivity value in most of the visible region.

Normally, the light from the waveguide gets coupled to nearby ring of the resonator due to their close proximity that results in evanescent coupling in between them. Due to this evanescent coupling, it will give rise to transfer of power from one to another. The arrangement of closed-loop designed via one ring waveguide and two straight waveguides kept in parallel acts as a resonator and allows accumulation of intensity at particular frequencies inside the structure. Regarding the visualization of the performance of the proposed ring resonators, a comprehensive simulation study has been done by means of MODE software. The MODE FDTD simulation tool involves various optimization modules concerning diverse application fields of optical devices.

Fig. 11 depicts the structure of the suggested optical ring resonator by a wave-guiding layer of CuO ring resonator. To explain the field spreading in the waveguides and for extracting the modes, primarily, the transverse electric (TE) and transverse magnetic (TM) modes for a 3D waveguide are examined, and the different properties of the wave guide are derived by Eigen mode Solver (EGM). The effective index method (EIM) conditions that initially a solution for the TE modes (or TM modes) is explicated via cross-section sight of the waveguides. Later the creation of ring resonator structural model, greater mesh accuracy is established for more correct results. Conversely by increasing the mesh accurateness more simulation data and a longer simulation time is spent. For the current analysis a simulation accuracy of 4 is set, the time for simulation is set to 5000 fs, the liner wave guide width is 500 nm, the thickness is 220 nm, the radius of the optical ring resonator is 5 μm and the opening between the ring and the straight waveguide is 100 nm. The incident light in the waveguide is in the TE mode and the wavelength analysis is from 300 to 900 nm. Moreover, in order to collect the field profile and power flow data in the frequency domain from the simulation results, energy monitors are set. Fig. 12 depict the mode field distribution of the waveguide for variable anneal time CuO resonator. It can be seen that energy is well confined in the resonator.

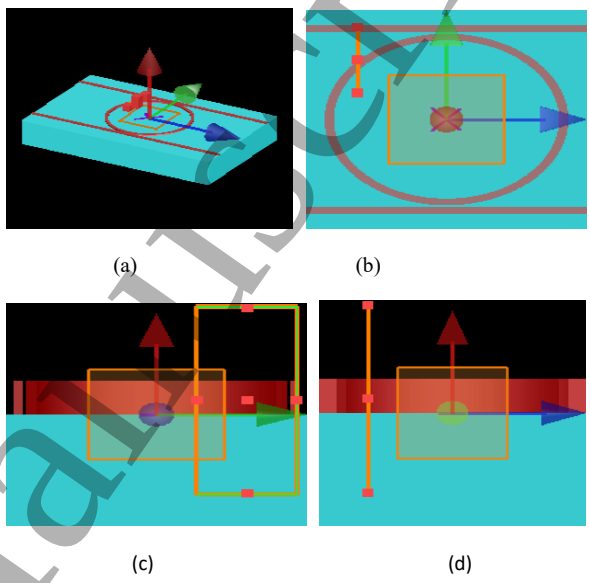

Fig. 11. Simulated structure of CuO coated ring resonator (a) 3D model of CuO ring resonator, (b) XY view, (c) YZ view and (d) XZ view

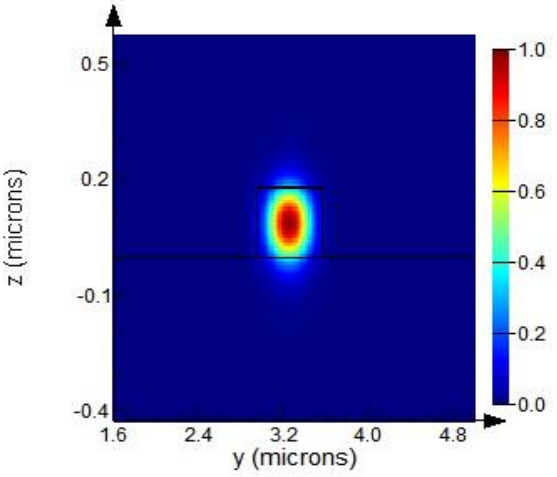

Fig. 12. The cross-section mode field distribution of a straight waveguide for CuO coated ring resonator.

3.3.2.1 Effective refractive index

Fig. 13 gives the plot of effective refractive indices of CuO (annealed at 5, 15, 25min) optical ring resonator. It

can be seen that effective refractive index (n_{ef}) for 15min annealed sample is highest at wavelength greater than 483nm. Whereas, for 5min annealed sample it is minimum for wavelength greater than 639nm. This can be described from the FESEM image of the CuO film. In 25min annealed sample there are big grains (i.e. more inter-grain spacing) present that allows the propagation of light very easily. However in 15min annealed sample the light speed is less and also they are more reflected as the grains are smaller, more ordered and condensed with fewer gaps. Thus, high n_{ef} permits light to be well-confined throughout the waveguide.

Now regarding the variation of effective refractive index (n_{ef}) with respect to the wavelength, the plot displays that on increasing the wavelength in the visible region, the n_{ef} diminishes. Effective refractive index is the fraction of light velocity in vacuum to mode velocity, for a given polarity in the path of transmission in a guiding structure (i.e. along the waveguide in the z-direction). Also the effective refractive index is the total refractive index of the optical resonator, depending on the mode with an addition of CuO film refractive index.

Since the refractive index of CuO that is used as a cladding material is dispersive i.e. changes with the wavelength and anneal time, therefore, accordingly n_{ef} will also vary with the wavelength variation.

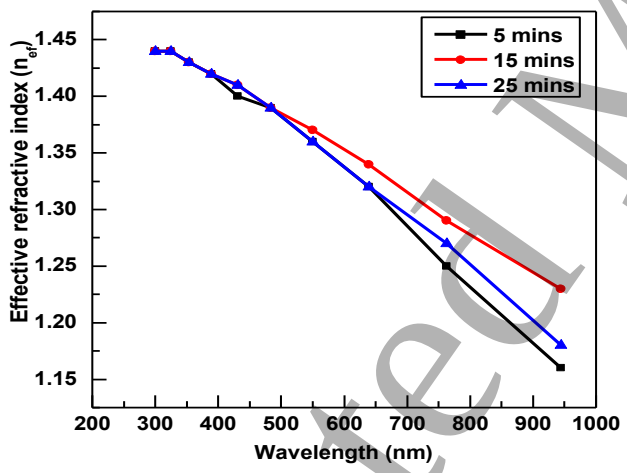

Fig. 13. Effective refractive index vs. wavelength for various anneal time CuO ring resonator

3.3.2.2 *Propagation Constant*

Fig. 14 depicts the variation of propagation constant 'β' against the wavelength. As we increase the wavelength range, 'β' declines in visible regime. It infers that increment in the wavelength range creates negative change in phase and amplitude. The reason can be mathematically clarified by the propagation constant relation with n_{ef} and wavelength 'λ' given in eq. 13 [35].

$$\beta = \frac{2\pi}{\lambda} n_{ef} \tag{13}$$

As we know, from the aforementioned variation in n_{ef} with respect to λ, that on increasing the range of wavelength there is considerable reduction in the value of n_{ef}. Since $\beta \propto n_{ef}$ and $\beta \propto 1/\lambda$ therefore it has an exponentially decrement curve against wavelength.

Now let us consider the effect of anneal time on the propagation constant. For the region below 350 nm, there is approximately zero effect of anneal time on the negative change in β against wavelength. And for the region above 350nm, 15min sample has the maximum propagation constant. The cause behind such behaviour can be recognized from the direct dependence of β on n_{ef}.

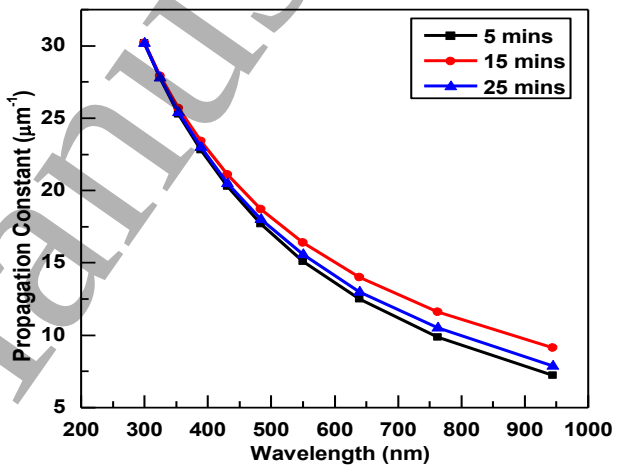

Fig. 14. Propagation constant vs. wavelength for various anneal time CuO ring resonator.

3.3.2.3 *Group velocity*

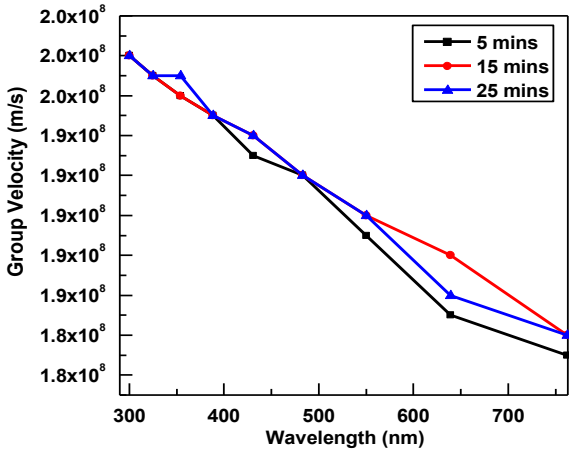

Fig. 15. Group velocity vs. wavelength for various anneal time CuO ring resonator.

Fig. 15 illustrates the dependency of group velocity on visible region wavelength. It was witnessed that below 550nm there is no such substantial alteration for different anneal time, whereas above 550nm, 15min shows the maximum group velocity among all. This infers that group delay, which has an inverse behaviour than group velocity, is less in 15min sample resonator. Therefore this behaviour of group velocity in CuO ring resonator enables a pathway for time-delay applications. Now, group velocity (v_g) of resonator can be related with the following given eq. 14.

$$v_g = \left(\frac{c}{n_{ef}}\right) \Big/ \left(1 - \frac{\lambda}{n_{ef}} \frac{dn_{ef}}{d\lambda}\right) \quad (14)$$

Therefore, the dependency of vg on nef may possibly be the reason for the relatable pattern depicted in fig. 15.

3.3.2.4 Loss

Optical losses in the resonator are common. Real resonator cannot be ideal as it certainly hold some imperfections. Fig. 16 illustrates the alterations in resonator losses with respect to wavelength. Loss increases with an increase of wavelength. It can also be observed that loss is less for 15min CuO among all, making it a suitable material for use in ring resonator wave-guiding layers. The rise in loss with increasing wavelength can be due to some absorption made by silicon core of the waveguide, scattering of lights at the core/cladding interface and the absorption of cladding material (CuO). In addition to this small dispersion and defects caused by the roughness of CuO film are also the reasons of loss. These losses are intrinsic that cannot be avoided and are difficult to control. The increment in the loss at higher wavelength connotes decrement in gain at higher wavelength.

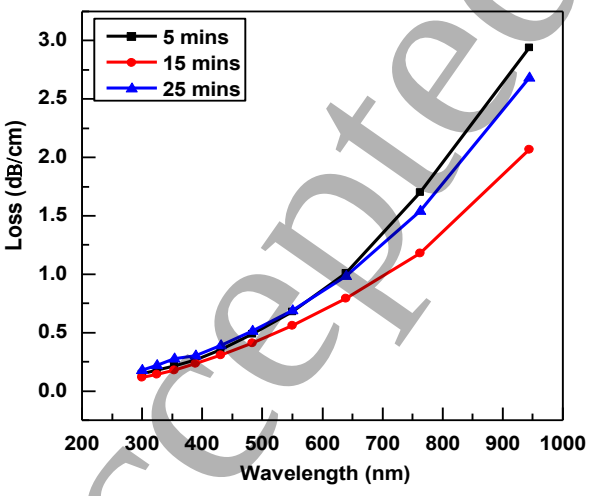

Fig. 16. Loss vs. wavelength for various anneal time CuO ring resonator.

3.3.2.4 Dispersion

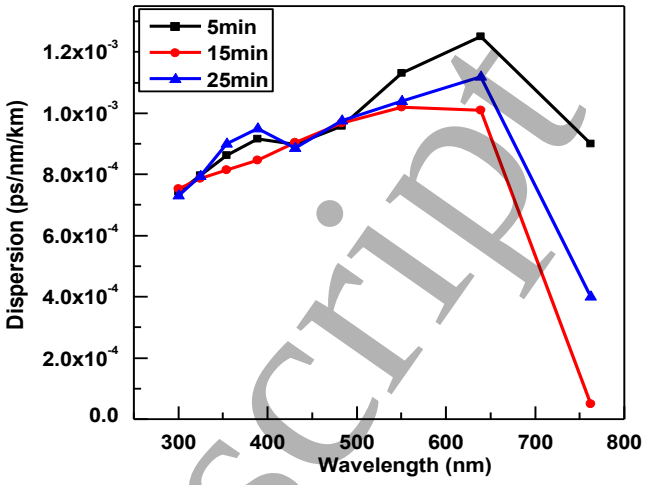

Fig. 17. Dispersion vs. wavelength for various anneal time CuO ring resonator.

Fig. 17 exemplifies the alterations in dispersion with respect to wavelength in CuO resonator. As there is a considerable change in refractive index of material with wavelength, therefore the signified dispersion is termed as material dispersion. As the mode group velocity is directly related to the refractive index, the several spectral components of a known mode will travel at dissimilar speeds, relying on the wavelength. Material dispersion is, thus, an intra-modal dispersion phenomenon, and is of certain meaning for single mode optical fibre. From the resultant dispersion spectra there is an insignificant change in all the cases below 500nm. Beyond 500nm, it can be predicted that there is a negative change in dispersion with increasing wavelength. This negative change tends the dispersion to approximately zero value at longer wavelength. Subsequently, we can observe that 15min annealed CuO resonator shows minimum material dispersion among all.

3.3.2.5 Transmission intensity

Since the reflectivity's of CuO film formed at different anneal time varies subsequently with wavelength, therefore, it will create a noteworthy impact on the transmission intensity of light ray (given in fig. 18). With such purpose we have scrutinized the transmission intensity of the light travelling through the CuO optical resonator. The radius of the ring resonator is taken as 5μm. Thus, round-trip for thousands order of magnitude will create resonance inside the whole system. At drop point we have obtained the transmission intensities for diverse anneal time in fig. 18. We can illustrate that transmission intensity is high at longer wavelength, whereas, it is less at shorter wavelength. Dependency of transmission intensity is on both dispersion and losses of

the resonator. At longer wavelength dispersion is very less (approximately zero) and losses are high, compared to shorter wavelength. Due to negligible dispersion, in visible region transmission intensity is high. This remarkable characteristic enables it for visible photonic applications. And since the losses are less in 15min annealed sample therefore it is making the most suitable characteristic among all.

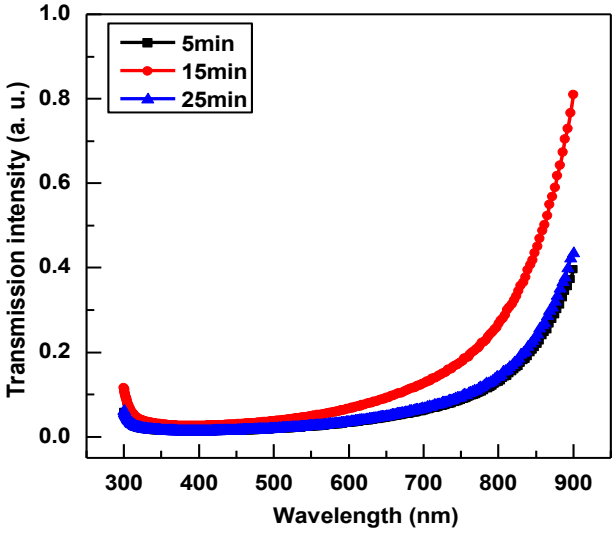

Fig. 18. Transmission intensity vs. wavelength graph for 5min, 15min and 25 min ring resonator.

Now we can resolute the resonance wavelength (λ_{Mo}) by considering the complete optical path length equivalent to an integral number of wavelengths (M_o) [5]

$$\lambda_{M_o} = \frac{2\pi r n_{grp}(\lambda)}{M_o} \tag{15}$$

here '$n_{grp}(\lambda)$' represents the group refractive index, 'M_o' the integer depicts the order of mode and 'r' specifies the CuO ring resonator radius. In order to deliberate the effective refractive index $n_{ef}(\lambda)$ of the microcavity that varies with wavelength (because of material property and the dispersion of waveguide), $n_{grp}(\lambda)$ has been incorporated in the eq. 15. Therefore, $n_{grp}(\lambda)$ can be specified as [36]

$$n_{grp}(\lambda) = n_{ef}(\lambda) - \frac{\partial n_{ef}(\lambda)\lambda}{\partial \lambda} \tag{16}$$

Here $n_{ef}(\lambda)$ and $n_{grp}(\lambda)$ in terms of operating wavelength λ_o is [5]

$$n_{ef}(\lambda) = n_{ef}(\lambda_o) + \frac{\partial n_{ef}}{\partial \lambda}(\lambda - \lambda_o) \tag{17}$$

$$n_{grp}(\lambda) = \frac{n_{ef}(\lambda_o)\lambda - n_{ef}(\lambda)\lambda_o}{(\lambda - \lambda_o)} \tag{18}$$

Further resonance wavelength can be derived by putting eq. 18 into eq. 15 [5].

$$\lambda_{M_o} = \frac{2\pi(r) \times \left[n_{ef}(\lambda_o)\lambda - n_{ef}(\lambda)\lambda_o\right]}{M_o(\lambda - \lambda_o)} \tag{19}$$

The potential capability of ring resonator and its applicability in the secured communication system can be illustrated by investigating some necessary constraints like free spectral range (FSR), full-width at half-maximum (FWHM), Quality factor (Q) etc.

3.3.2.6 Free Spectral Range (FSR)

FSR can be defined as the spacing between two consecutive resonant peaks that can be related with group refractive index as given below in eq. 20 [5].

$$FSR = \frac{\lambda^2}{2\pi n_{grp}(\lambda) \times (r)} \tag{20}$$

In fig. 19 influence of changing inverse radius (1/r) on FSR has been graphically represented. The response of 5min, 15min and 25min exemplifies that there is a noteworthy effect of radius on the resonator performance. It can be seen that for all the cases there is an increment in FSR with 1/r variation. It is the consequence of the dependency of group refractive index (n_{grp}) on the ring radius. The n_{grp} of a material is the fraction of light's velocity in vacuum to the light's group velocity in medium. Also from eq. 17 it can be said that n_{grp} has a direct relation with $n_{ef}(\lambda)$. As the ring radius is lessened the bending effect arises that manifests the shift of optical mode distribution in the direction of external waveguide sidewall. This creates an intersection between lateral roughness and optical distribution that could intensify the optical losses. This interaction influences the effective refractive index of the resonator vastly [37] and thus affects the group refractive index.

Additionally, it can be observed that CuO cladding material based ring resonator is demonstrating less FSR when compared with the reported works illustrated in table. VII. Also, among 5min, 15min and 25min annealed CuO film, 15min shows the lowest FSR. The FSR is the space between two consecutive transmission peaks. Small FSR often confines the frequency range of operation. However, large FSR leads to larger bandwidth, and as a consequence, deprived spectral resolution. For favourable communication, bandwidth is a big matter of concern. Maximum transmission in less bandwidth is acceptable.

Thus, it can be said that 15min annealed CuO resonator has better FSR among all other.

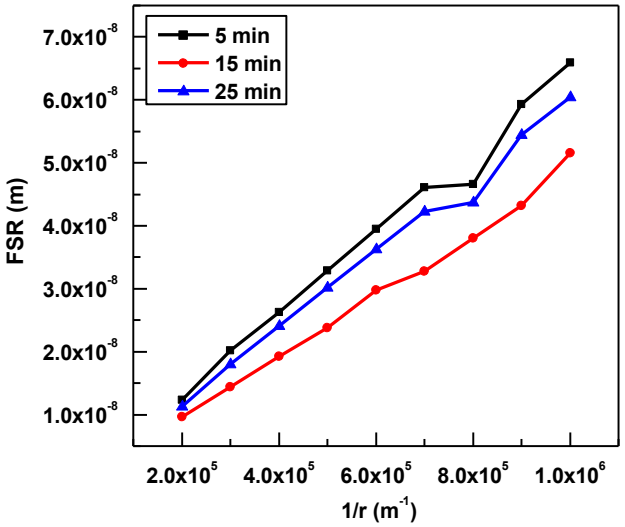

Fig. 19. Deviation in FSR of a CuO ring resonator with respect to the inverse of its radius.

3.3.2.6 Full-width at half-maximum (FWHM)

Now FWHM can be derived for the resonance spectral range of the CuO ring resonator using eq. 21 [38].

$$FWHM = \frac{K^2\lambda^2}{2\pi^2 r n_{grp}(\lambda)} \quad (21)$$

here K=1 gives the intrinsic loss of ring. Now FWHM and FSR can be related as provided in eq. 23.

$$FWHM = \frac{FSR}{\pi} \quad (22)$$

FWHM of the ring resonator symbolises the sharpness of the resonance spectrum. From fig. 20, 15min has least FWHM with inverse radius of resonator ring (1/r) among all, in the given wavelength range. It implies that for 15min sample has less sharpness in peaks with respect to wavelength. The reason can be attributed from the mathematical expression given in eq. 22 that gives the relation between FSR and FWHM.

Moreover we can observe from table. VII that CuO cladding material based FWHM is very less when compared to other reported work. This low value of FWHM decreases the strain and optical losses in the cavity that enhances the finesse. Finesse is basically the ratio of FSR to FWHM that totally relies on the reflectivity of the cladding material. High finesse in the optical cavities results in repressed dissipation rate of photons decay and large power circulation in the cavity that would ultimately augment the quality factor of the device.

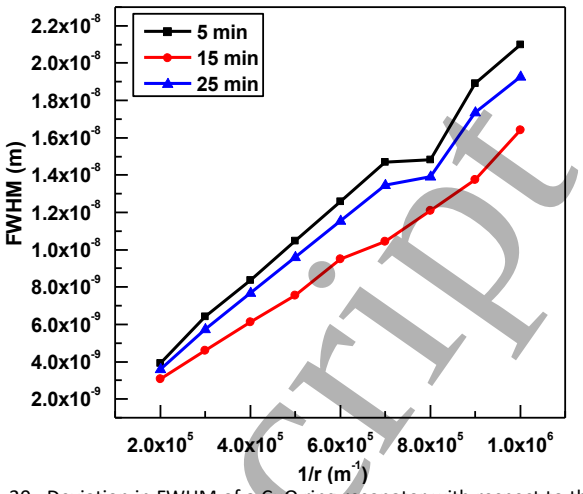

Fig. 20. Deviation in FWHM of a CuO ring resonator with respect to the inverse of its radius.

3.3.2.7 Quality factor

Quality factor is an important parameter to be inspected so as to get the perceptiveness of the resonance spectrum of CuO ring resonator. Also it helps to understand the bandwidth and shape of the optical fiber response. The quality factor can be related with FSR and FWHM as given below [39].

$$Q = \frac{n_{grp}(\lambda)2\pi(r)\times FSR}{\lambda \times FWHM} \quad (23)$$

It can also be written as [5]

$$Q = \frac{\lambda}{FWHM} = \frac{\lambda\pi}{FSR} \quad (24)$$

Fig. 21 gives the variation of quality factor with respect to 1/r, which is the most obligatory parameter to be known. It can be seen that Q factor decreases with increment in 1/r.

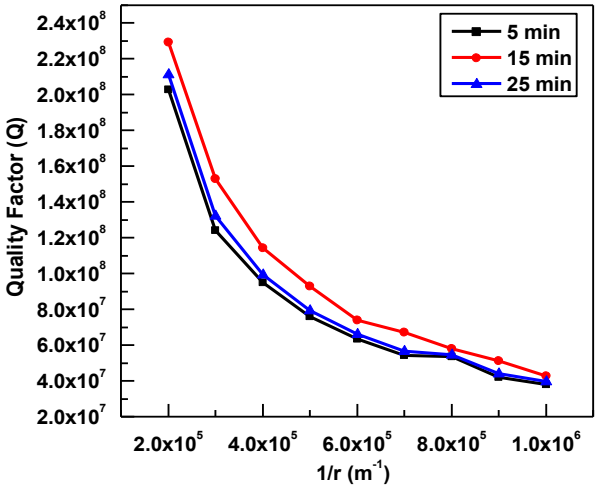

Fig. 21. Deviation in Quality factor of a CuO ring resonator with respect to the inverse of its radius.

Scientifically, the reason behind the variation in Q-factor is due to the changes in its structural parameter. Since we have varied the ring radius, therefore, n_{ef} will change vastly as it is highly dependent upon the distance between the ring and straight waveguide. Due to the change in n_{ef} there would be the huge variation in resonant wavelength that ultimately indicates the device sensitivity or quality factor of the resonator [40]. Mathematically Q depends upon FWHM with inverse factor. As FWHM is increasing with decreasing ring radius, the quality factor will increase for the same. Moreover, the Q factor is highest for 15min and lowest for 5min. This denotes that comparatively losses are less in 15min annealed CuO film that can be validated from fig. 16.

High quality factor in 15min CuO indicates low power consumption and long lifetime of the photons. But simultaneously, it limits the injection and extraction of optical power from the ring, which inflicts a fundamental optical restriction on the speed of the device. This may possibly be moderated by using resonators with lower Q, but at the expense of device efficiency. Therefore, anneal time variation is giving a platform to control the Q factor of the resonator according to the application.

Furthermore we have compared cladding material performance used in the present work with the reported work for 3.1 μm ring radius in table. VII, and the relevant parameters such as loss and quality factor with the reported resonators in table. VIII.

TABLE VII

Comparison of CuO cladding ring resonator with other cladding ring resonators for 3.1μm ring radius

SN	Cladding Material	FSR (nm)	FWHM (nm)	Finesse	Quality Factor
1	Benzene [41]	41.09	28.2	1.46	0.050×10^3
2	Propanol [41]	41.65	26.25	1.58	0.053×10^3
3	Methane [41]	41.07	25.75	1.59	0.054×10^3
5	5min annealed CuO	21.51	6.89	3.12	$2*10^8$
6	15min annealed CuO	15.27	4.77	3.20	$2.3*10^8$
7	25min annealed CuO	19.45	6.12	3.18	$2.1*10^8$

TABLE VIII

Comparison of CuO resonator properties with other reported resonators

S. N.	Resonator Material	Loss in dB/cm	Quality Facor
1.	TiO2	7.5 (ring radius= 150μm)	$1.6*10^5$ [42]
2.	Etched Silicon	3-4 (ring radius= 5μm)	$(2*10^5)$-$(3*10^5)$ [43]
3.	Silicon	0.9 (ring radius= 51.5μm)	$7.6*10^5$ [44]
4.	Er doped ZnO	7.8 (ring radius= 5μm)	400 [5]
5.	3C-silicon carbide (SiC)-on-insulator (SiCOI)	2.9 (ring radius= 40μm)	$1.42*10^5$ [45]
6.	5min annealed CuO	2.9 (ring radius= 5μm)	$2*10^8$
7.	15min annealed CuO	2.68 (ring radius= 5μm)	$2.3*10^8$
8.	25min annealed CuO	2.07 (ring radius= 5μm)	$2.1*10^8$

4. Conclusion

Effectively we have deposited CuO film at diverse anneal time by means of sol–gel spin-coating method on n-Si substrate. The optical and structural properties have been thoroughly discussed via XRD, FESEM, AFM, UV-Vis Spectroscopy, PL and Ellipsometry instruments. On the basis of diverse anneal time, it was found that among all, 15min sample has the finest capability to reflect more amount of light. The highly reflective surface of CuO film empowered this material in visible photonic resonator applications. Consequently, we have proposed CuO film (for different anneal time) coated ring resonators and Fabry-Perot resonators. The ring resonator was simulated and examined via MODE Solution simulation tool. And the results of Fabry-Perot were examined via MATLAB tool. The transmission intensities for different annealed samples have been presented and deliberated in detail. The transmission intensity with varying anneal time demonstrated the effect of surface roughness. For CuO Fabry-Perot resonator, the transmission intensity revealed the plausibility to use this proposed device in secured optical communication system. Additionally, the contrast factor and finesse at different anneal time and angle of light incidence have been theoretically represented for CuO Fabry-Perot resonator. Whereas, in CuO ring resonator, we have theoretically found the FSR, FWHM and quality factor for 5min, 15min and 25min sample CuO film ring resonator, and compared them with the reported literatures. The result unveiled that 15min has the highest Q-factor that corroborates the consistency of the proposed device.

References

[1] Vahala Kerry J., "Optical microcavities," Aug. 2003, nature, vol. 424, no. 6950, pp. 839.

[2] Xiao Yun-Feng and Gong Qihuang, Jan. 2016, "Optical microcavity," fundamental physics to functional photonics devices, Science Bulletin, vol. 61, no. 3, pp. 185-186.

[3] Wade James H. and Bailey Ryan C., March 2016, "Applications of optical microcavity resonators in analytical chemistry," Annual Review of Analytical Chemistry, vol. 9, pp. 1-25.

[4] Wang Qiang et al., Oct. 2017 "A novel ultra-thin-walled ZnO microtube cavity supporting multiple optical modes for bluish-violet photoluminescence, low-threshold ultraviolet lasing and

microfluidic photodegradation," NPG Asia Materials, vol. 9, no.10, pp. e442.

[5] Agarwal Lucky, Naik B. Naresh and Tripathi Shweta, Oct. 2017, "Highly reflective Er-doped ZnO thin-film coating for application in a UV optical ring resonator," Nanotechnology, vol. 28, no. 46, pp. 465707.

[6] Ge Li, Feng Liang and Schwefel Harald GL, Dec. 2017, "Optical microcavities: new understandings and developments," Photonics Research, vol. 5, no. 6, pp. OM1-OM3.

[7] Passaro Vittorio et al., Nov. 2012, "Recent advances in integrated photonic sensors," Sensors, vol. 12, no. 11, pp. 15558-15598.

[8] Altmann Konrad, Jan. 2018, "Embedding the photon with its relativistic mass as a particle into the electromagnetic wave," Optics express, vol. 26, no. 2, pp. 1375-1389.

[9] Kobayashi Tetsuro, June 2012, "Experimental studies of completely closed optical cavities enclosed with total-internal-reflection walls," Optics express, vol. 20, no. 14, pp. 16033-16038.

[10] Li Feng, 2013, "Fabrication and characterization of ZnO-based microcavities working in the strong coupling regime: polariton laser," Dissertation, University Nice Sophia Antipolis.

[11] Lin Shiyun et al., Jan. 2008, "Luminescence enhancement by Si ring resonator structures on silicon on insulator," Applied Physics Letters, vol. 92, no. 2, pp. 021113.

[12] Zhang Zhang et al., March 2019, "A new route for fabricating polymer optical microcavities," Nanoscale.

[13] El-Trass A. et al., Nov. 2011, "CuO nanoparticles: synthesis, characterization, optical properties and interaction with amino acids," Applied Surface Science, vol. 258, no. 7, pp. 2997-3001.

[14] Ray Sekhar C., 2001, "Preparation of copper oxide thin film by the sol–gel-like dip technique and study of their structural and optical properties," Solar energy materials and solar cells vol. 68, pp. 307-312.

[15] Chen George Y. et al., 2017, "Photodetector with photothermal cascaded Fabry-Perot etalons," 25th Optical Fiber Sensors Conference (OFS), IEEE.

[16] Hadjaj F., Belghachi A., Halmaoui A., Belhadj M., Mazouz H., 2013, "Study of a Fabry-Perot Resonator," World Academy of Science, Engineering and Technology, International Journal of Physical and Mathematical Sciences, vol. 7, no. 12.

[17] Sun Yuze and Fan Xudong, 2011, "Optical ring resonators for biochemical and chemical sensing," Analytical and bioanalytical chemistry, vol. 399, no. 1, pp. 205-211.

[18] Singh Satyendra Kumar et al., 2016, "Performance analysis of RF-sputtered ZnO/Si heterojunction UV photodetectors with high photo-responsivity," Superlattices and Microstructures, vol. 91, pp. 62-69.

[19] Akgul Funda Aksoy et al., 2014, "Influence of thermal annealing on microstructural, morphological, optical properties and surface electronic structure of copper oxide thin films," Materials Chemistry and Physics, vol. 147, no. 3, pp. 987-995.

[20] Shrividhya, T., et al., 2014 "Determination of structural and optical parameters of CuO thin films prepared by double dip technique." Journal of Materials Science: Materials in Electronics, vol. 25, no. 9, pp. 3885-3894.

[21] Chandrappa, K. G., and T. V. Venkatesha, 2013, "Generation of nanostructured CuO by electrochemical method and its Zn–Ni–CuO composite thin films for corrosion protection." Materials and corrosion, vol. 64, no. 9, pp. 831-839.

[22] Lee, Jung Eun, et al., 2018, "Deposition and characterization of Cu (In, Ga) Se2 thin films from the ink of sonochemically prepared CIGSe nanoparticles." Chinese journal of physics, vol. 56, no.1, pp. 392-403.

[23] Saravanan R. et al., 2013, "Visible light induced degradation of methylene blue using CeO2/V2O5 and CeO2/CuO catalysts," Materials Science and Engineering: C, vol. 33, no. 8, pp. 4725-4731.

[24] Stil I. et al., 2012, "Loss of WR10 waveguide across 70–116 GHz," Proc. 22nd Int. Symp, Space Terahertz Technol.

[25] Jaberansary Ehsan et al., 2013, "Scattering loss estimation using 2-D Fourier analysis and modeling of sidewall roughness on optical waveguides," IEEE Photonics Journal, vol. 5, no. 3.

[26] Vlasov Yurii A. and McNab Sharee J. , 2004, "Losses in single-mode silicon-on-insulator strip waveguides and bends," Optics express, vol. 12, no. 8, pp. 1622-1631.

[27] Yap Kuan Pei et al., 2009, "Correlation of scattering loss, sidewall roughness and waveguide width in silicon-on-insulator (SOI) ridge waveguides," Journal of Lightwave Technology, vol. 27, no. 18, pp. 3999-4008.

[28] Agarwal Lucky et al., 2016, "Fabrication and characterization of Pd/Cu doped ZnO/Si and Ni/Cu doped ZnO/Si Schottky diodes," Thin Solid Films, vol. 612, pp. 259-266.

[29] Akgul Unal, Yildiz Koksal and Atici Yusuf, 2017, "Influence of annealing time on the physical properties of reactively sputtered CuO thin film," Journal of Materials Science: Materials in Electronics, vol. 28, no. 6, pp. 4758-4762.

[30] Ismail Nur et al., 2016, "Fabry-Pérot resonator: spectral line shapes, generic and related Airy distributions, linewidths, finesses, and performance at low or frequency-dependent reflectivity," Optics express, vol. 24, no. 15, pp. 16366-16389.

[31] Stone J. and Stulz L. W., 1987, "Pigtailed high-finesse tunable fibre Fabry-Perot interferometers with large, medium and small free spectral ranges," Electronics letters, vol. 23, no. 15, pp. 781-783.

[32] Lee Seung-Hyun, 2001, "Confocal Fabry-Perot Cavity," SUNY at Stony Brook University.

[33] Ring Resonators: Theory and Modeling. In: Integrated Ring Resonators, 2007, Springer Series in Optical Sciences, vol 127, Springer, Berlin, Heidelberg.

[34] Fahrenfort J., 1961, "Attenuated total reflection: A new principle for the production of useful infra-red reflection spectra of organic compounds," Spectrochimica Acta, vol. 17, no. 7, pp. 698-709.

[35] De Leonardis, Francesco, Richard A. Soref, and Vittorio MN Passaro. "Investigation of Electric Field Induced Mixing in Silicon Micro Ring Resonators." Scientific reports 7.1 (2017): 3401.

[36] Tsigaridas Georgios N. , 2017, "A study on refractive index sensors based on optical micro-ring resonators," Photonic Sensors, vol. 7, no. 3, pp. 217-225.

[37] Bogaerts Wim et al. , 2012, "Silicon microring resonators," Laser & Photonics Reviews, vol. 6, no. 1, pp. 47-73.

[38] Little Brent E. et al. , 1997, "Microring resonator channel dropping filters," Journal of lightwave technology, vol. 15, no. 6, pp. 998-1005.

[39] Khan M. J. et al., 1999, "Mode-coupling analysis of multipole symmetric resonant add/drop filters," IEEE Journal of Quantum Electronics, vol. 35, no. 10, pp. 1451-1460.

[40] Ling, Tao, and L. Jay Guo., 2013, "Sensitivity enhancement in optical micro-tube resonator sensors via mode coupling." Applied Physics Letters, vol. 103, no. 1, pp. 013702.

[41] Ariannejad, M. M., Elnaz Akbari, and Iraj S. Amiri, 2018, "Micro-ring resonator made by ion exchange technique and detecting benzene (C6H6), propanol (C3H7OH) and methane (CH4) as cladding layer." Laser Physics, vol. 28, no. 10, pp. 106201.

[42] Evans, Christopher C., Chengyu Liu, and Jin Suntivich, 2015, "Low-loss titanium dioxide waveguides and resonators using a dielectric lift-off fabrication process." Optics express, vol. 23, no. 9, pp. 11160-11169.

[43] Xiao, Shijun, et al., 2007, "Compact silicon microring resonators with ultra-low propagation loss in the C band." Optics express, vol. 15, no. 22, pp. 14467-14475.

[44] Griffith, Austin, et al., 2012, "High quality factor and high confinement silicon resonators using etchless process." Optics express, vol. 20, no. 19, pp. 21341-21345.

[45] Fan, Tianren, et al., 2018, "High Q Integrated Photonic Microresonators on 3C SiC-on-Insulator Platform." CLEO: Science and Innovations. Optical Society of America.